Performance of an oxy-polishing step in the 100 kWth chemical looping combustion prototype

Chemical Engineering Journal 409 (2021) 128202

Contents lists available at ScienceDirect

Chemical Engineering Journal

journal homepage: www.elsevier.com/locate/cej

Performance of an oxy-polishing step in the 100 kW_{th} chemical looping combustion prototype

Daofeng Mei [a,b,*], Carl Linderholm [a], Anders Lyngfelt [a]

[a] Division of Energy Technology, Department of Space, Earth and Environment, Chalmers University of Technology, Gothenburg SE-41296, Sweden
[b] College of Engineering, Huazhong Agricultural University, Wuhan 430070, China

ARTICLE INFO

Keywords:
Chemical looping combustion
Oxy-polishing
Post-oxidation chamber
Solid fuel
Manganese ore
Overall oxygen ratio

ABSTRACT

Unconverted fuel gases are normally present in the gas leaving the fuel reactor of a Chemical Looping Combustion (CLC) process. Depending on several factors, including oxygen carrier and fuel volatiles content, the unconverted gases represent 5–30% of the oxygen needed for full combustion. Further conversion of these fuel components is imperative to achieve adequate combustion and to fulfill the requirements for CO_2 storage. An oxy-polishing step using highly concentrated O_2 to fully oxidize the fuel components offers a straightforward one-step way to reach complete combustion. However, systematic and detailed investigation is lacking while it is essential for design, scale up and optimization. In this work, the oxy-polishing is studied in a post-oxidation chamber (POC) of a 100 kW_{th} unit using different solid fuels and manganese ores in the CLC process. With various flows of air as oxidation agent, the POC performance was evaluated under stable operations in a wide range of operating conditions. An overall oxygen ratio was defined to analyze the effect of O_2 excess in the POC. Experimental results show that the oxidation of fuel gas from the fuel reactor can be greatly enhanced by air entering the POC, with the gas conversion being improved from 87 to 90% before the POC to as high as 99–100% after the POC. Full oxidation in POC can be accomplished with excess of O_2. For the cases of incomplete oxidation, CO was normally found in higher concentrations than CH_4. In a few cases close to optimum, CO and O_2 simultaneously have normalized concentrations below 0.5–1% with a low overall oxygen ratio of around 1.01. The POC performance was further compared to the results from a simple reactor model.

1. Introduction

The mean atmospheric CO_2 concentration has been continuously rising after the pre-industrial decades, which is widely acknowledged as a major factor to the global warming. To limit the temperature increase within a reasonable level, elimination of CO_2 emission is imperative [1]. Chemical Looping Combustion (CLC) is a technology which can generate power with the feature of intrinsic CO_2 capture [2–6], thus avoiding the associated high energy penalty for a CO_2 separation step. Solid fuels, such as coal and biomass, are more extensively studied in CLC, due to their abundance and high accessibility [3,7], while gas and liquid fuels are also feasible in this process [8–12]. A simplified CLC system is basically composed of an air reactor, a fuel reactor and oxygen carrier particles circulating between the two reactors [11,13], as depicted in Fig. 1. In the fuel reactor, the solid fuel is decomposed to volatiles and char via reaction (R1), while the char is gasified to CO and H_2 via reaction (R2). The oxygen carrier, a metal oxide with MeO_x as the oxidized form, supplies oxygen for the combustion of volatiles and gasification products in reaction (R3). The reduced oxygen carrier, in the form of $MeO_{x\text{-}1}$, is then conveyed to the air reactor to recover to the initial form via reaction (R4). The gas leaving the fuel reactor is mainly comprised of CO_2, H_2O and minor other components (e.g. S- and N-based species), where CO_2 can be captured by simple condensation of steam using a condenser. Thus, CLC is a combustion technology with low energy penalty for CO_2 capture [2,3,14]. To date, >3700 h of operation with solid fuels have been successfully demonstrated in continuous CLC units with a nominal thermal power of 0.5 kW_{th} to 3 MW_{th} [2–4,15–19]. Great progress has been achieved in oxygen carrier development, reaction kinetics, modeling and reactor design [3,7,20–26], while there are still some challenges to be faced and addressed [4,27].

Fuel reactor:

$$\text{Solidfuel} \rightarrow \text{Char} + \text{Volatiles} \quad \text{(R1)}$$

* Corresponding author at: Division of Energy Technology, Department of Space, Earth and Environment, Chalmers University of Technology, Gothenburg SE-41296, Sweden.
E-mail address: daofeng.mei@chalmers.se (D. Mei).

https://doi.org/10.1016/j.cej.2020.128202
Received 9 October 2020; Received in revised form 14 December 2020; Accepted 16 December 2020
Available online 30 December 2020

Nomenclatures

a	example of the first variable for uncertainty analysis
b	example of the second variable for uncertainty analysis
c	example of the third variable for uncertainty analysis
ASU	air separation unit
CLC	chemical looping combustion
CSTR	continuous stirred-tank reactor
f	target function to be calculated, with $f = f(a, b, c, \ldots)$ being a, b, and c the measured parameters
$F_{air,j}$	volumetric flow of air entering reactor j (j = AR or POC), $L_N \cdot s^{-1}$
$F_{CO,i}$	molar flow of CO at the inlet (i = in) or outlet (i = out) of the POC reactor, $mol \cdot s^{-1}$
$F_{i,j}$	molar flow rate for gas i ($i = CH_4$, CO, CO_2, H_2, or O_2) at the outlet of reactor j (j = FR or POC), $mol \cdot s^{-1}$
MeO_x	oxygen carrier in oxidation state
$MeO_{x\text{-}1}$	oxygen carrier in reduced state
m_{FR}	fuel reactor solids inventory per MW_{th} thermal power, $kg \cdot MW_{th}^{-1}$
POC	post-oxidation chamber
t	time, min
T_{FR}	fuel reactor temperature, °C
$T_{POC,i}$	temperature at the inlet (i = in) or outlet (i = out) of the POC reactor, °C
$x_{i,j}$	concentration of gas i ($i = CH_4$, CO, CO_2, H_2, or O_2) in reactor j (j = FR, AR or POC)
$x_{i,N}$	normalized concentration of gas i ($i = CH_4$, CO, CO_2, H_2, or O_2) at the outlet of POC
$\Omega_{OD,j}$	oxygen demand at the outlet of reactor j (j = FR or POC)
$\eta_{gas,j}$	gas conversion in reactor j (j = FR or POC)
$\lambda_{O,overall}$	overall oxygen ratio considering fuel reactor and POC
σ_i	absolute standard deviation of variable i ($i = a, b, c, \ldots$)

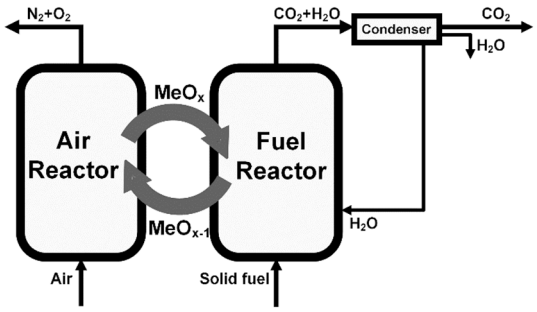

Fig. 1. Schematic diagram of CLC technology using a solid fuel.

$$\text{Char} + H_2O \rightarrow CO + H_2 + \text{Ash} \quad \text{(R2)}$$

$$\text{Volatiles}, CO, H_2 + MeO_x \rightarrow MeO_{x-1} + CO_2 + H_2O \quad \text{(R3)}$$

Air reactor

$$MeO_{x-1} + 1/2O_2 \rightarrow MeO_x \quad \text{(R4)}$$

One challenge for CLC is the incomplete combustion of fuel gases (mainly CH_4, CO and H_2) at the fuel reactor exit, mainly caused by insufficient contact of oxygen carrier particles and fuel gases, as a consequence of bubbling effect in fluidization systems [2,3,27]. These unconverted fuel components usually correspond to an oxygen demand of 5–30%, as defined in *Section 3.1* below, although there are also examples of 100% combustion using more expensive oxygen carrier materials [3]. The higher oxygen demand means more energy penalty for oxygen production, therefore, several strategies have been theoretically analyzed with models [28–30] and experimentally investigated with different reactor configurations [31–36] by taking the advantages of faster reaction kinetics under various conditions [28,37–41], higher reactivity of oxygen carrier [42–44] and better mixing between fuel gas and oxygen carrier particles [31,45]. The results from pilot operation indicate that a fully converted gas is difficult to achieve at reasonable costs. Thus, the gas must be further converted, e.g. by gaseous O_2. Therefore, it is expected that an optimized full-scale CLC plant would not have full combustion in the fuel reactor [6], which would be unacceptable for good system performance and to fulfill the requirements for CO_2 transport and storage [2,27], if not properly addressed. Consequently, the effluent flue gas from fuel reactor needs to be further converted with methods leading to a combustion close to 100%, to get a better system performance as well as to have almost pure CO_2 stream for storage.

The post-oxidation step, also called oxy-polishing, uses highly concentrated gaseous O_2 to burn the residual fuel components from the fuel reactor. It is a straightforward one-step way to reach full combustion [46], which can address the described problems. The oxygen amount required in oxy-polishing step can be adjustable, which makes the CLC system more flexible for different fuels and operation conditions. In the oxy-polishing step, the unburnt combustibles, including gas components (CH_4, H_2 and CO) and elutriated char (mainly carbon) from fuel reactor, are directly converted to CO_2 and H_2O via the exothermic oxidation reactions (R5) to (R8) by an external flow of O_2 gas. The gaseous O_2 stream can be from an Air Separation Unit (ASU) using mature cryogenic technology [47]. Therefore, only a post-oxidation chamber and an ASU unit could be enough for the oxy-polishing step. In this case, full combustion with 100% CO_2 capture can be realized in the CLC process without the development and use of complex systems. Meanwhile, the heat released during the combustion of the unconverted fuel-reactor residual fuel components can be recovered by using a heat exchanger. The total energy penalty for gaseous O_2 generation in oxy-polishing step is at a comparably low level [6,7,48], because the required amount of O_2 is relatively quite low. Thus, in the case of a CLC system with 90% gas conversion, the added energy penalty will be only around 0.6% units [7].

$$CH_4 + 2O_2 \rightarrow CO_2 + 2H_2O \quad \Delta H^0 = -802.3\ kJ \cdot mol^{-1} \quad \text{(R5)}$$

$$H_2 + 1/2O_2 \rightarrow H_2O \quad \Delta H^0 = -241.8\ kJ \cdot mol^{-1} \quad \text{(R6)}$$

$$CO + 1/2O_2 \rightarrow CO_2 \quad \Delta H^0 = -282.9\ kJ \cdot mol^{-1} \quad \text{(R7)}$$

$$C + O_2 \rightarrow CO_2 \quad \Delta H^0 = -393.5\ kJ \cdot mol^{-1} \quad \text{(R8)}$$

Although the oxy-polishing concept for CLC has been proposed in early publications [6,46], the systematic and detailed study of this technology is still lacking, while it is essential for design, scale up and optimization. Few works were performed on the oxy-polishing process [49–52] to examine the feasibility for further improving the combustion. In those works, the oxy-polishing was tested in a post-oxidation chamber (POC) using air or pure O_2, downstream of the fuel reactor. According to those preliminary tests, the oxygen demand after the POC was decreased to 2.5% from 18% before the POC at 860 °C for the 100 kW_{th} system located at Chalmers University of Technology [49,50], meaning further improvement is needed. The oxy-polishing step was also tested by several cases in a 1 MW_{th} unit erected at Technische Universität Darmstadt under partial CLC conditions, i.e. combustion in the fuel reactor was partly assisted by air flow [51], or full CLC conditions [52].

Complete combustion of those residual fuel components can be accomplished using a high flow rate of air or O_2 to the POC. However, the connection and the interrelation of the POC performance and the fuel reactor behavior was not fully explored, which would be important for getting a better system efficiency and a high CO_2 capture. The flow of O_2 to oxy-polishing step should be carefully studied to help to find out the optimal ratio of O_2 injection, because it is directly linked to the cost for oxygen generation and the purity of the CO_2 stream.

The present work explores the performance of the oxy-polishing step by using a POC reactor in a 100 kW_{th} CLC unit, which can contribute to the design and scale up of an oxy-polishing reactor in large CLC systems. Stable operations were achieved in the 100 kW_{th} unit by using three fuels and two manganese ores under different temperatures, fuel rates and oxygen carrier circulations, which produced various fuel compositions at the inlet of POC. These different cases, in combination with the change of air flow to the POC, resulted in a wide range of influencing factors for the behavior of POC. By comparing the gas composition at the inlet and outlet of the POC, an improved combustion was always reached, whereas a dependence on fuel reactor gas types was also found. Under conditions close to optimum, simultaneous low concentration of different combustibles was detected at the outlet of POC, which is encouraging for the scale up of oxy-polishing technology.

2. Experiments and simulation

2.1. Oxygen carriers

Two manganese ores were involved in the experimentation, which were denoted as SC and Sinaus, respectively, according to their as-received forms and origin/suppliers. The SC was a calcined (identified by "C") manganese ore supplied by Sibelco (identified by letter "S") company. The Sinaus was an Australian (identified by "aus") manganese ore, where the term "Sin" indicated its sintered state in supply. These manganese ores were extensively used in the 10 and 100 kW_{th} pilot CLC units in previous works [2,17,49], which showed good reactivity and physical properties. The ore particles received were mainly composed of Mn, Fe, Si and Al elements with a Fe/Mn molar ratio of 0.1 and 0.2 for SC and Sinaus, respectively [17,49]. Minor fractions of alkali, e.g. around 1 wt% K element, were also present in the fresh material, which could act as a catalyst favoring the gasification of char, thus, to reach a better combustion [43,53]. The manganese ores were crushed and sieved to smaller than 355 μm, ready for use in the 100 kW_{th} unit. Some of the physical properties of these oxygen carrier particles are summarized in Table 1. The bulk density was determined following an ISO standard funnel method [54] by pouring an amount of particles to a cylinder container with a determined volume, which is important for the estimation of a suitable velocity of fluidization gas in the reactors of the CLC unit. The sieved oxygen carrier materials have an average particle size of d50 = 185 μm for SC and 175 μm for Sinaus, respectively, which was determined by sieving a weighted amount of particles through a series of stainless-steel standard sieves. The crushing strength of the particles was the average value for fracturing the 30 randomly selected particles, which was determined by a digital apparatus (FGN-5, Shimpo) and took a value of 3.2 and 3.5 N for SC and Sinaus, respectively. Attrition index of the manganese ore particles was determined at room temperature using a customized jet cup rig [55,56]. The attrition indexes of SC and Sinaus are 1.37 and 1.21 wt%·h^{-1}, respectively, which in combination with the high crushing strength suggest their suitability for applying in fluidization systems [55,57].

Table 1
Physical properties of SC and Sinaus manganese ores.

	SC	Sinaus
Bulk density (kg·m^{-3})	1840	2090
Median size, d50 (μm)	185	175
Crushing strength (N)	3.2	3.5
Attrition index (wt.%·h^{-1})	1.37	1.21

2.2. Solid fuels

Steam cured biomass "black pellets" provided by Arbaflame from Norway, a type of wood char from Schütte in Germany, and a type of Colombian coal from Calenturitas mine, which were designated as BP, GWC, and CAL, respectively, were used as fuels for the tests performed in the 100 kW_{th} unit. These solid fuels were crushed and sieved to a median size of d50 = 1800, 250 and 130 μm for BP, GWC and CAL, respectively, before the experiments. Here, the median size of the fuel particles was determined with the same method for the oxygen carriers, as stated in the previous section. The proximate and ultimate analysis of the solid fuels were determined following an ISO and an ASTM standard method [58,59], respectively. As seen in Table 2, the BP pellets are a high-volatile biomass fuel, while the GWC wood char and CAL coal have significantly lower volatiles. The heating value of BP is lower than that of the other two fuels, which can be related to its lower carbon content and higher oxygen fraction. Thus, a higher flow rate of fuel would be expected for BP than GWC and CAL to reach the same thermal power.

2.3. Operation conditions in the 100 kW_{th} system

In previous publications, details about the 100 kW_{th} prototype were well documented [50,60], where more information can be found. The system is featured by a circulating fluidized-bed fuel reactor and a high efficiency 4-chamber carbon stripper located between the fuel and air reactor. These designs allow a long residence time of char inside the fuel reactor and an efficient separation of char and oxygen carrier in the carbon stripper, thus the loss of char to air reactor was minimized [18,60]. Experimental tests were conducted with two manganese ores, i.e. SC and Sinaus, and three solid fuels, i.e. BP, GWC and CAL, under various operation conditions, as seen in Table 3. The main variables during steady operations are the air flow rate to air reactor, $F_{air,AR}$, and the thermal power input, P_{th}, which were changed in the range of 28–42 $L_N \cdot s^{-1}$ and 42–85 kW_{th}, respectively, depending on the types of fuel and oxygen carrier, see Table 3. The variation of air flow to the air reactor is made to reach different solids circulation, since the latter is controlled by the air flow [61]. With the change of air flow, the solids circulation was varied, which resulted in the change of fuel reactor temperature, T_{FR}, in a small interval of 960–970 °C. Except for that, the other operation parameters, such as air reactor temperature and fluidization gas flow, were kept roughly constant under stable operations. The fuel reactor, loop seals and carbon stripper were all fluidized with steam, while the fuel tank and pressure measuring ports along the reactor were usually swept with known flow rates of N_2. Gas from the outlet of the fuel reactor was first led to a condenser to remove the moisture and then to a gas analysis unit to determine the composition at room temperature. The concentration of CH_4, CO, CO_2, H_2 and O_2 were measured by an online gas analyzer (NGA2000, Rosemount ^{TM}) and registered with a data logger at a rate of one point per second. This gas analyzer can determine the concentration of CH_4, CO, CO_2 and O_2 in the range of 0-100 vol% and the concentration of H_2 within 0-20 vol%. The air-reactor gas was cooled down and analyzed by another analyzer (Sick Maihak, SIDOR) to determine the fractions of CO, CO_2 and O_2 within a range of 0-20 vol%, 0-5 vol% and 0-25 vol%, respectively. These determined gas concentrations in combination with the known amounts of N_2 entering the reactors were later used to calculate the molar flow rate of the measured gas component.

2.4. Post-oxidation chamber (POC)

Downstream of the cyclone of the fuel reactor, the gas was led to the POC for further combustion of fuel gases and/or char particles from the fuel reactor, see Fig. 2. The POC was a vertically situated cylindrical tube

Table 2
Proximate and ultimate analysis of the solid fuels used in this work.

	Proximate (wt.%, ar)				Ultimate (wt.%, daf)					LHV[a] (MJ·kg^{-1})
	FC[b]	V	M	A	C	H	N	S	O[c]	
BP	18.7	74.2	6.9	0.3	53.5	6.0	0.1	0.0	40.3	18.7
GWC	76.4	15.7	5.1	2.8	88.1	2.7	0.5	0.0	8.6	29.3
CAL	53.1	29.4	11.0	6.5	78.3	6.6	1.6	0.8	12.7	24.6

[a] lower heating value, [b] fixed carbon, [c] by difference

Table 3
Main operation conditions of the 100 kW$_{th}$ reactor.

Oxygen carrier	Fuel	P_{th} (kW$_{th}$)	$F_{air,AR}$ (L$_N$·s^{-1})	$F_{air,POC}$ (L$_N$·s^{-1})	Reference
SC	BP	67	28–42	0–6.7	[17]
SC	GWC	80	28–42	0.8–6.7	[17]
SC	GWC	42	38–42	1.7–3.3	[17]
SC	GWC	67	42	0.8–1.7	[17]
SC	CAL	85	28–42	0–5	[17]
Sinaus	BP	67	28–38	0–5	–
Sinaus	BP	51	38	0–3.3	–
Sinaus	GWC	55	33–42	0–5	[49]
Sinaus	CAL	65	28–42	0–6.7	[49]

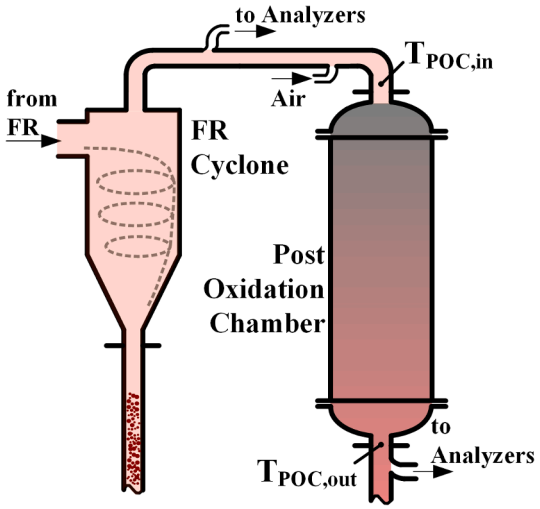

Fig. 2. Sketch of the POC connecting the 100 kW$_{th}$ fuel reactor cyclone.

with an inner diameter of 0.30 m and a length of 1.50 m, which was manufactured with high-temperature-resistant steel and insulated by ceramic blankets to minimize the heat loss. The temperatures at the inlet and outlet of POC were continuously monitored by a K-type thermal couple. Instead of pure O_2, in this work air was used as an oxidation agent in the POC for safety considerations. This air flow was split into two tangential streams at the injection port to enhance the mixing of air and combustibles. Concentrations of CO, CO_2 and O_2 at the POC outlet were measured by a gas analyzer (Sick Maihak, SIDOR) in the range of 0-20 vol%, 0-100 vol% and 25 vol%, respectively, and acquired every second by a data logger.

There were no external heating elements for the POC, thus its temperature was determined by the gas stream entering this reactor, the exothermic reactions (R5)-(R8) and heat losses from the POC wall. The variation of POC temperature was mainly affected by the air flow rate entering the POC, $F_{air,POC}$, which was varied in the range of 0–6.7 L$_N$·s^{-1} to facilitate the evaluation under different operation conditions, see Table 3.

2.5. POC simulation

Gas composition from the fuel reactor can be used in a zero-dimensional model composed of a series of continuous stirred-tank reactor (CSTR) to simulate the oxy-polishing process. Three interconnected CSTRs with an identical volume were used for the simulation to have a reasonable comparison with the POC experiments. The elutriated char from the fuel reactor was not included in the simulation, because its flow cannot be correctly calculated. An open-source tool, Cantera [62], coupled with MATLAB® codes was employed to perform the simulation, while the reaction mechanism and kinetics were described by detailed intermediate and elementary steps of the oxidation reactions of the fuel (i.e. CH_4, CO and H_2) using the GRI-Mech 3.0 package [63]. Given the inlet gas-mixture composition and reaction conditions, the zero-dimensional model can calculate the gas composition leaving each CSTR, while the effluent from the last one was considered for comparisons with the POC results. This model, after a validation with experiments, could be useful for guiding future scale-up design of the POC subsystem in a CLC unit.

3. Data evaluation

3.1. Calculations

The molar flow rate, F_j with a unit of mol·s^{-1}, of the gas leaving the fuel reactor (j = FR) or the POC (j = POC) was calculated in Eq. (1) based on N_2 flow, $F_{N2,j}$, entering these reactors. Using a known molar flow of N_2 and the concentration, $x_{i,j}$ (vol.%), of component i (i = CH_4, CO_2, CO, H_2 or O_2) in the effluent gas stream, the total gas molar flow rate can be determined for each reactor.

$$F_j = \frac{F_{N_2,j}}{1 - \sum x_{i,j}} \quad (1)$$

Then, the molar flow rate of gas component i in reactor j can be obtained in Eq. (2) using the total molar flow F_j calculated from Eq. (1) and the gas concentration $x_{i,j}$.

$$F_{i,j} = x_{i,j} \cdot F_j \quad (2)$$

With the concentration, $x_{i,j}$ (i = CO, CH_4, H_2 or CO_2), at the outlet of reactor j, a dimensionless oxygen demand, $\Omega_{OD,j}$, representing the theoretical ratio of O_2 required for complete oxidation of residual combustibles [18] can be calculated by Eq. (3).

$$\Omega_{OD,j} = \frac{0.5x_{CO,j} + 2x_{CH_4,j} + 0.5x_{H_2,j}}{\Phi_0(x_{CO,j} + x_{CH_4,j} + x_{CO_2,j})} \quad (3)$$

where the Φ_0 represents the stoichiometric moles of O_2 per mole carbon for fully burning the fuel, being calculated as Φ_0 = 1.05, 1.05 and 1.19 for BP, GWC and CAL fuels, respectively.

According to the values of oxygen demand, the gas conversion in reactor j, $\eta_{gas,j}$, which reflects how far or close from complete conversion of gaseous combustibles [49] to CO_2 and H_2O, can be easily obtained as Eq. (4).

$$\eta_{gas,j} = 1 - \Omega_{OD,j} \quad (4)$$

Specific solids inventory, m_{FR}, in the fuel reactor, with the unit of

kg·MW$_{th}^{-1}$, which represents the mass of oxygen carrier particles per MW$_{th}$ fuel [49], can be estimated by Eq. (5) using the measured pressure drop of the fuel reactor, Δp_{FR} (Pa), and the thermal power input, P_{th} (kW$_{th}$).

$$m_{FR} = \frac{A_c}{g} \cdot \frac{\Delta p_{FR}}{P_{th}} \cdot 10^3 \quad (5)$$

where A_c (m^2) is the geometric inner cross-section area of the fuel reactor tube and g (m·s^{-2}) refers to the gravitational acceleration.

To make a comparison for the results from different operation conditions, the concentration of component i (i = CH$_4$, CO, H$_2$ or O$_2$) at POC outlet was normalized by the total gaseous carbon fraction using Eq. (6).

$$x_{i,N} = \frac{x_{i,POC}}{(x_{CH_4} + x_{CO} + x_{CO_2})_{POC}} \quad (6)$$

A new parameter, namely overall oxygen ratio ($\lambda_{O,overall}$), was defined to evaluate the relation of full combustion and excess of O$_2$ in the POC. As seen in Eq. (7), the total oxygen provided by the oxygen carrier in the fuel reactor and the air to the POC was calculated by the two numerators with the concentration of O$_2$, CO$_2$, CO and H$_2$ from the POC and the theoretic oxygen ratio Φ_0 for the fuel. Thus, the value of $\lambda_{O,overall}$ can be calculated as the ratio of the above obtained total oxygen and the stoichiometric oxygen for full fuel combustion determined by the denominators.

$$\lambda_{O,overall} = \frac{(x_{O_2} + x_{CO_2} + 0.5x_{CO} - 0.5x_{H_2})_{POC}}{\Phi_0 (x_{CO_2} + x_{CO} + x_{CH_4})_{POC}} + \frac{\Phi_0 - 1}{\Phi_0} \quad (7)$$

where the Φ_0 and x_i represent the stoichiometric moles of O$_2$ per mole carbon for fully burning the fuel and the measured concentration of component i (i = CH$_4$, CO, CO$_2$, H$_2$ or O$_2$) at the outlet of POC, as explained in Eq. (3) and Eq. (6), respectively.

3.2. Uncertainty analysis

Gas concentration in the stream from reactors is the basis for calculating the above-mentioned parameters. The uncertainty associated with the measuring apparatus can propagate to the calculation results and lead to some errors in the values. For different gas analyzers used in this work, the accuracy of each gas component is summarized in Table 4, according to the technical data provided by the manufacturer. Except for that, these analyzers can have some significant drifts as a function of week, even under normal use. To minimize this, the gas analyzers were calibrated every day before the experiments.

With the uncertainty shown in Table 4, the relative errors of calculation results from above equations can be estimated through the formula for uncertainty propagation in Eq. (8), assuming f as the target to be calculated, which has a known relation of $f = f(a, b, c, \ldots)$ with the measured variables, e.g. a, b, c, etc. Here, these measured variables can be the gas concentration obtained from the 100 kW$_{th}$ unit operation, while the f can be the terms on the left side of the above equations.

$$error = \frac{1}{f} \cdot \left\{ {\sigma_a}^2 \cdot \left(\frac{\partial f}{\partial a}\right)^2 + {\sigma_b}^2 \cdot \left(\frac{\partial f}{\partial b}\right)^2 + {\sigma_c}^2 \cdot \left(\frac{\partial f}{\partial c}\right)^2 + \cdots \right\}^{0.5} \cdot 100\% \quad (8)$$

where the symbol σ_i ($i = a, b, c, \ldots$) represents the absolute standard deviation of variable i, which, in the case of gas component, was calculated by multiplying the full-scale measuring range of the component, as seen in Section 2.3 and Section 2.4, with the uncertainty in Table 4, e.g. $\sigma_{CO} \leq \pm 1\%$, $\sigma_{CO2} \leq \pm 1\%$ and $\sigma_{H2} \leq \pm 0.2\%$, for the CO, CO$_2$ and H$_2$, respectively, from the fuel reactor.

For instance, to estimate the uncertainty of F_j in Eq. (1), the differential equation for each $x_{i,j}$ must be derived first. Using the measured $x_{i,j}$, the values of F_j and $\partial F_j / \partial x_{i,j}$ can be calculated, which together with the uncertainty of the measurement for $x_{i,j}$ in Table 4 were used to get the relative error of F_j by Eq. (8). For the parameters involved in this work, typical uncertainties are summarized in Table 5. In most of the cases, the errors are low in the range of $\leq \pm 2.3$–7.5%, which suggests a good reliability of these calculations. However, some relevant uncertainty, e.g. $\leq \pm 17.5\%$ for gas conversion in the POC, was also obtained, mainly due to the relatively lower concentrations of fuel components.

Table 4
Uncertainty of various components for different reactors.

	CH$_4$	CO	CO$_2$	H$_2$	O$_2$
Fuel reactor	$\leq \pm 1\%$	$\leq \pm 1\%$	$\leq \pm 1\%$	$\leq \pm 1\%$	$\leq \pm 1\%$
Air reactor	–	$\leq \pm 2\%$	$\leq \pm 2\%$	–	$\leq \pm 1\%$
POC	$\leq \pm 2\%$	$\leq \pm 2\%$	$\leq \pm 2\%$	–	$\leq \pm 1\%$

4. Results

4.1. Gas composition after the fuel and air reactors

Stable operation was easily achieved using the two manganese ores and the three solid fuels during the experiment. As an example, Fig. 3 depicts the gas concentration from fuel reactor, air reactor and the air flow entering the air reactor as a function of fuel feed time, using the SC ore and CAL coal. Rapid increase of CO$_2$ concentration to around 45 vol % for the fuel reactor was seen after the fuel started. At the same time, a continuous decrease of O$_2$ concentration in the air reactor was noticed until around t = 30 min, as the reduced oxygen carrier from fuel reactor was being oxidized in the air reactor. It is also noticed that there was a small CO$_2$ peak in air reactor in the initial minutes, which could be explained by that the initial temperature was insufficient for fast char gasification in the fuel reactor and carbon stripper, i.e. T_{FR} less than 845 °C. In this case, a loss of a small amount of char to air reactor occurred. After that, the temperature was always high enough for fast char conversion in the fuel reactor and carbon stripper, i.e. $T_{FR} > 925$ °C, thus no CO$_2$ or CO was observed at the air reactor exit after around t = 50 min. The concentration of CO$_2$ from the fuel reactor was increased from 45 to 57 vol% as the air reactor air flow was changed from 34 to 42 L$_N$·s^{-1}, which was accompanied by a slight drop of CO, H$_2$ and CH$_4$ concentration. An increase of air flow improves the fuel reactor performance because of a higher circulation rate of oxygen carrier between the air and fuel reactors [61], which also raises the solids inventory in the fuel reactor. Thus, more oxygen carrier particles were transported into the fuel reactor at higher air flows, which led to a better contact of fuel gases and the oxygen carrier. Despite this, the O$_2$ concentration of the air reactor was not greatly changed in the interval of 10-15 vol%, indicating that the reduction extent of the SC ore was relatively stable. When the fuel feed was stopped at around t = 135 min, the concentration of CO$_2$, CO, H$_2$ and CH$_4$ fell gradually to zero, while the O$_2$ in air reactor was recovered to its initial concentration. For the other fuels, i.e. BP and GWC, and manganese ores, i.e. SC and Sinaus, similar results were also obtained for the fuel and air reactors of the 100 kW$_{th}$ unit.

4.2. Gas composition after the POC

As the air was injected, the oxidation of the fuel-reactor gas was started in the POC, which is illustrated by the switching of air flow from $F_{air,POC}$ = 0 to 5 L$_N$·s^{-1} at around t = 6.6 min in Fig. 4. As displayed in Fig. 4, the concentration of CO and CO$_2$ began to decrease from 3.8 to 0 vol% and from 53 to 26 vol%, respectively, as the air flowed into the POC. There was a delay of approximately 0.5 min for gas concentration after switching the air flow from 0 to 5 L$_N$·s^{-1}, which was caused by the distance between the sampling port and the gas analyzers. An O$_2$ concentration of around 3.8 vol% was detected after the POC, which indicates the air injected to the POC was excessive. Although more moles of CO$_2$ were expected by the oxidation of CO, CH$_4$ and char, a lower CO$_2$ concentration was actually detected after the injection of air, which was a result of the dilution by the 4 L$_N$·s^{-1} N$_2$ in the air.

Table 5
Typical relative errors of different parameters in this work.

F_{FR}	F_{POC}	$F_{i,FR}$	$F_{i,POC}$	$\eta_{gas,FR}$	$\eta_{gas,POC}$	$x_{i,N}$	$\lambda_{O,overall}$
≤ ±7.0%	≤ ±5.3%	≤ ±7.5%	≤ ±6.3%	≤ ±6.3%	≤ ±17.5%	≤ ±5.4	≤ ±2.3%

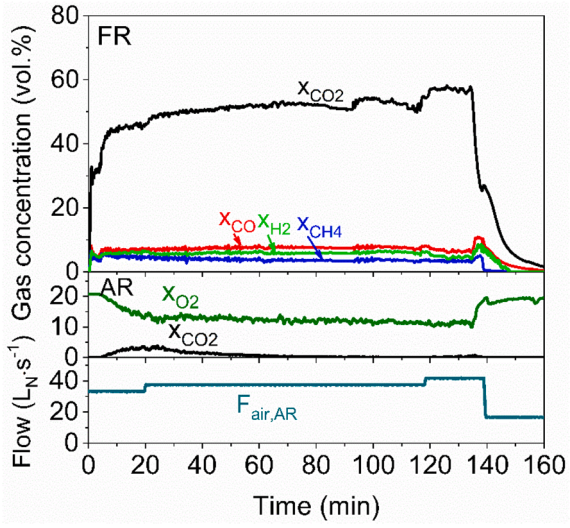

Fig. 3. Concentration x_i of CO_2, CO, H_2 and CH_4 for the fuel reactor (FR) as well as CO_2 and O_2 for the air reactor (AR), and the flow rate of air entering AR, $F_{air,AR}$, as a function of fuel feed time, using the SC ore as oxygen carrier and 85 kW_{th} CAL coal as fuel; $t = 0$ corresponds to fuel start.

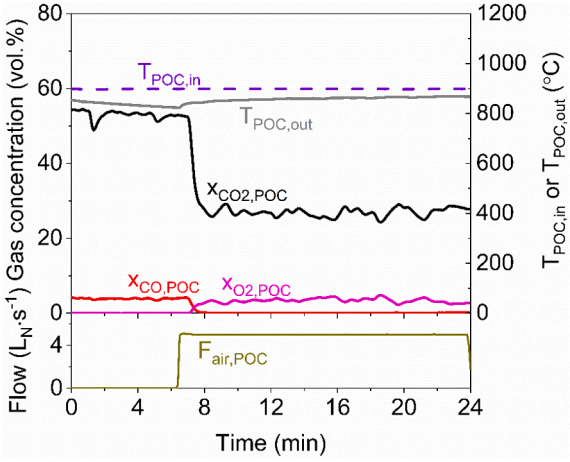

Fig. 4. Typical progress in POC gas concentration and temperature for switching the air flow, $F_{air,POC}$, from 0 to 5 $L_N \cdot s^{-1}$ during the combustion of GWC wood char with Sinaus manganese ore, fuel thermal power was 55 kW_{th}.

As aforementioned, the POC chamber has no external heating elements, which means that it was heated by the hot gas stream from the fuel reactor and the heat released by the exothermic oxidation reactions. As seen in Fig. 4, the temperature at the inlet, $T_{POC,in}$, was rather stable, whereas the outlet temperature was lower due to heat loss from the wall and the cooling effect by air injection. After starting air addition at around $t = 6.6$ min, the temperature at the POC outlet was gradually increased from 825 to 875 °C, mainly attributable to the exothermic oxidation of the combustibles, see reactions (R5)-(R8).

4.3. Gas flow after the fuel reactor and POC

Molar flow rates of gas components calculated for the fuel reactor (CO_2, CO, H_2 and CH_4) and the POC (CO_2, CO, O_2 and CH_4 in some cases) are plotted as a function of time for comparison purposes, as seen the example in Fig. 5. For the use of BP pellets, stepwise declines of gas flows for the fuel reactor are noticed in the first 27 min in Fig. 5(a). This phenomenon was a result of malfunction of a 3-way valve connecting the fuel reactor exit, purge N_2 and gas analyzers. In that period, unquantifiable flows of N_2 were directed to the analyzers, thereby incorrect gas flows for fuel reactor were obtained for the first 27 min. However, the POC measurement worked well, thus the gas flow from POC can be correctly calculated, as seen in Fig. 5(a). In the initial minutes, the POC temperature was gradually increased from 700 to 850 °C, which resulted in a faster kinetics for CO oxidation and thus lowering the CO flow. After $t = 27$ min, stable concentrations were achieved both for the fuel reactor and the POC under various flows of air to POC and air reactor. The concentration of CH_4 for POC was measured after around $t = 80$ min, which can reflect the oxidation degree of volatiles [64,65]. As seen in Fig. 5(a), a flow of CH_4 and CO close to zero was calculated between $t = 80$ and 125 min, indicating a full oxidation of CO and CH_4 in POC. The unmeasured H_2 can also be assumed to reach a full conversion in this case, considering its higher reactivity than CO and CH_4. Decreasing the POC air flow to less than 6.8 $L_N \cdot s^{-1}$ resulted in an insufficient oxidation of fuel components, therefore, increases in CO and CH_4 flows were seen when the air flow was reduced.

In the combustion of GWC wood char, extremely low CH_4 flow was observed from fuel reactor during the entire period of fuel feed, because of the low volatiles content in this fuel, see Table 2. As seen in the first 150 min of Fig. 5(b), both CO and CH_4 were absent after POC, while the CO_2 flow was higher for the POC than fuel reactor. This means full oxidation was reached at POC during the first 150 min. Additionally, in the period of $t = 118$–134 min, there was an abrupt increase of O_2 flow and a decrease of CO_2 flow leaving the POC due to a temporary air ingress to the gas analyzing system. After around $t = 150$ min, the fuel thermal power was increased from 42 to 67 kW_{th}, thus higher gas flows for CO_2, CO and CH_4 components were calculated at the fuel reactor and POC exit.

In the case of CAL coal combustion, there was no air flowing to the POC during the first 54 min in Fig. 5(c), meaning no oxidation of the fuel components occurred in the POC. Therefore, similar flows of CO and CO_2 were found for the fuel reactor and the POC in this period, while the H_2 and CH_4 from POC were not measured. The gradual increases of CO and CO_2 flows for both reactors as well as H_2 flows for the fuel reactor during the first 54 min are related to a faster char gasification, as the fuel reactor temperature was increased from 845 to 925 °C (not shown in the figure). Despite this, the CH_4 flow from the fuel reactor was quite stable, which could be attributed to a roughly constant devolatilization rate of the CAL coal in this temperature interval. After around $t = 54$ min, a 1.8 $L_N \cdot s^{-1}$ air was injected into the POC, which led to drastic increases of CO_2 and CO flows at POC exit. The sum of CO_2 and CO flow from POC was notably higher than the total flow of CO_2, CO and CH_4 from the fuel reactor, i.e. 0.13 versus 0.09 $mol \cdot s^{-1}$, which can be explained by the oxidation of char elutriated from the fuel reactor [50]. Furthermore, since the complete oxidation was not achieved, it can be said that the O_2 supplied with the 1.8 $L_N \cdot s^{-1}$ air was inadequate for full oxidation. Under a higher POC air flow of 3.3 $L_N \cdot s^{-1}$, some decreases of CO flow were seen, however, the complete oxidation was still not reached albeit some excess O_2 were observed. This behavior might be caused by several factors, such as not enough reaction time, low temperature and inadequate mixing of char and O_2, however, it is not clear which is the dominant reason. At around $t = 140$ min, the fuel flow was effectively cut off, thus the molar flows of CH_4, CO, CO_2 and H_2 were gradually

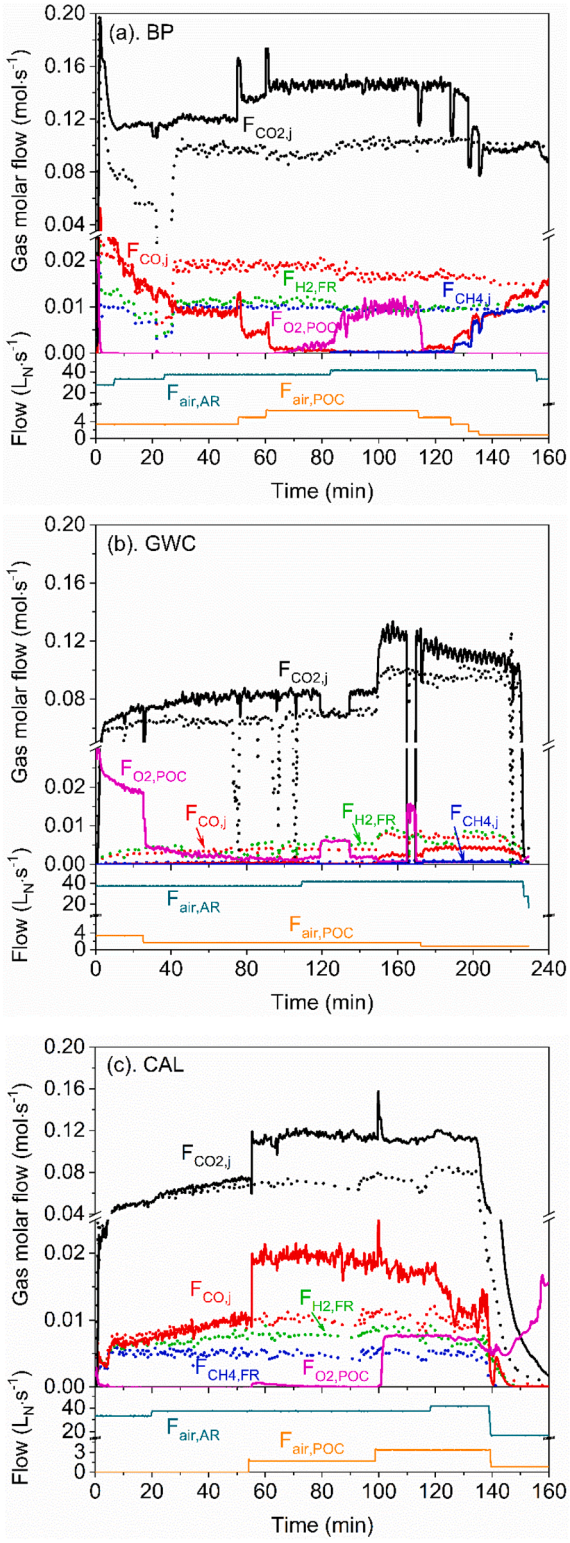

Fig. 5. Comparison of gas molar flow $F_{i,j}$ ($i = CO_2$, CO, H_2, CH_4 or O_2) at the outlet of fuel reactor (j = FR) and POC (j = POC) for (a) BP pellets, (b) GWC wood char with the change of thermal power from 42 to 67 kW_{th} at around $t = 150$ min and (c) CAL coal, using SC manganese ore as oxygen carrier; Solid lines for POC exit (j = POC) and dot lines for fuel reactor exit (j = FR), under various $F_{air,AR}$ and air flow rate $F_{air,POC}$; No measurements of H_2 for all the cases, CH_4 was measured after around $t = 80$ min for BP and during the entire period for GWC; Data from three examples of tests in Table 3.

reduced to zero. The continuous increase of O_2 flow after the fuel stop was a result of switching to fluidization with air.

Consequently, further oxidation of combustibles can be realized in the POC of the 100 kW_{th} unit, resulting in more CO_2 in the effluent gas stream. Some of the combustibles contain a significant fraction of char elutriated from the fuel reactor, which can be oxidized to CO and/or CO_2 in the POC. The char elutriated from fuel reactor was caused by the low riser height, the low efficiency of the cyclone in this small-scale CLC unit as well as by the type and particle size of fuel [49].

4.4. Improvement on gas conversion

The gas conversion - $\eta_{gas,FR}$ and $\eta_{gas,POC}$ for fuel reactor and POC, respectively- are plotted as a function of air flow rate to the air reactor in Fig. 6 for GWC wood char and Sinaus manganese ore. As mentioned before, a better contact between oxygen carrier and fuel gases can be realized at higher air reactor flows, thus higher gas conversions in fuel reactor are expected under higher air flows to the air reactor [61]. This principle is also applicable to the POC with a constant air injection rate, hence positive effect of air reactor flow on the gas conversion in POC is also seen in Fig. 6. The improvement on gas conversion with the use of POC is shown for the pair of "Sinaus + GWC" using a constant air flow to the POC. In this case, most of the combustibles from the fuel reactor were converted when the POC was in use, leading to a gas conversion of 0.993–0.997 compared to 0.887–0.894 after the fuel reactor, thus a great improvement on combustion was attained. By using the Sinaus + GWC pair, the oxygen demand after the POC can be decreased to 0.3–0.7% in comparison to 10.6–11.3% after the fuel reactor.

4.5. Effect of POC air flow

Increasing the POC air flow can result in more available O_2 in the POC as well as a higher temperature at the outlet of POC, due to the exothermic nature for the oxidation of combustibles, see reactions (R5)-(R8). In this case, more CO_2 and less CO were obtained at the POC outlet as shown in Fig. 7(a), in the light of faster reaction kinetics at higher temperatures from 830 to 980 °C and higher O_2 availability. Complete oxidation of CO was reached with $F_{air,POC} > 5$ $L_N \cdot s^{-1}$, while an O_2 flow of 0.008 $mol \cdot s^{-1}$ was found at POC exit. The quite stable inlet temperature, $T_{POC,in}$, in Fig. 7(a) was a result of steady fuel reactor operation. For the combustion of CAL coal, the cases became a bit different in Fig. 7(b), where the values of the parameters shown are increasing as a function of POC air flow. The continuous increase of $T_{POC,in}$ in Fig. 7(b) can be considered as a result of the stabilization for fuel reactor operation, which was also a function of time. This parameter would affect the temperature of POC and thus the reaction between O_2 and combustibles.

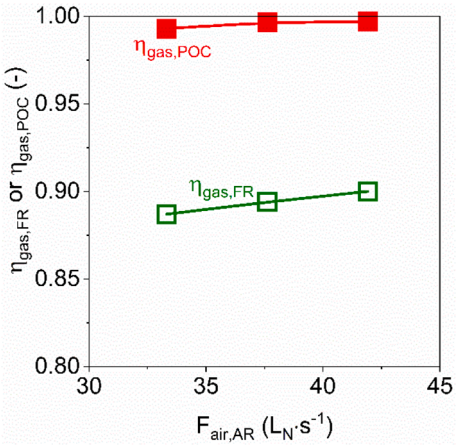

Fig. 6. Gas conversion in the POC ($\eta_{gas,POC}$) and the fuel reactor ($\eta_{gas,FR}$) for the "oxygen carrier + fuel" pair of "Sinaus + GWC" using $F_{air,POC} = 5.0$ $L_N \cdot s^{-1}$.

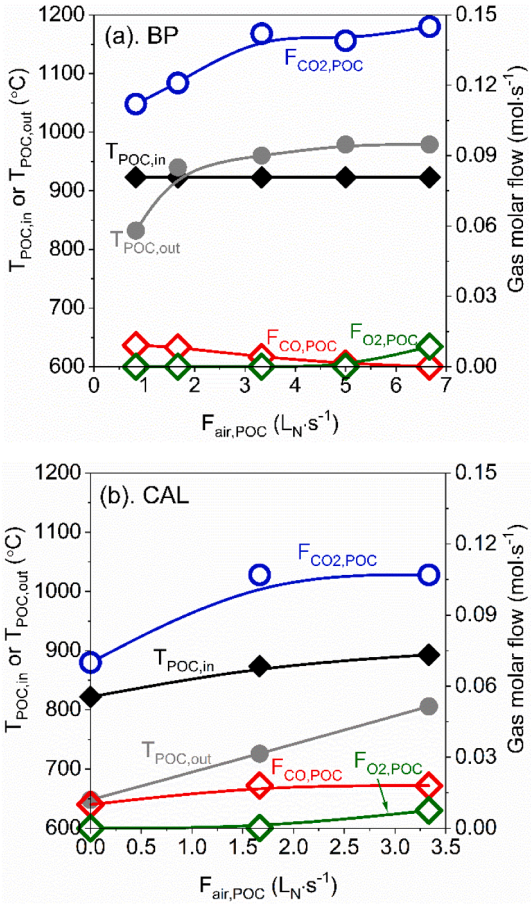

Fig. 7. Temperature at the inlet, $T_{POC,in}$, and the outlet, $T_{POC,out}$, of POC reactor and molar flows of CO_2, $F_{CO2,POC}$, and CO, $F_{CO,POC}$, as a function of POC air flow, $F_{air,POC}$, for the combustion of (a) 67 kW_{th} BP pellets and (b) 85 kW_{th} CAL coal using the SC manganese ore.

It should also be notable that the POC air flow was rising at the same period, which provides more O_2 for oxidation. Therefore, the higher CO_2 flow in Fig. 7(b) obtained at POC outlet can be ascribed to both higher air flow and higher temperature. At the same time, it was also observed that the CO flow at POC exit was slightly increased in Fig. 7(b), which can be caused by the insufficient oxidation of coal char elutriated from the fuel reactor [49], although a surplus oxygen of 0.007 mol·s^{-1} was detected using a POC air flow of 3.3 L_N·s^{-1}. This phenomenon was absent in Fig. 7(a), due to a much lower rate of elutriation for biomass char than coal char, i.e. 0–3% and 7–14%, respectively, according to a material balance calculation [50].

4.6. Trade-off between full oxidation and oxygen excess

Oxygen entering the POC with the air injection can contribute to the oxidation of various combustibles, of which CO was used as an indicator to evaluate the behavior of the POC. The molar ratio $(F_{CO,out}/F_{CO,in})_{POC}$ taking into account the flows of CO at the outlet, $F_{CO,out}$, and inlet, $F_{CO,in}$, of POC is plotted as a function of POC air flow in Fig. 8. In line with the previous discussions, it is generally found that a lower $(F_{CO,out}/F_{CO,in})_{POC}$ was reached at a higher POC air flow. Despite this, oxygen at the POC outlet can always be found (excepting $F_{air,POC} = 0$), especially for the full oxidation case, which means a pure CO_2 stream could not be achievable in this case. Thus, a trade-off would be expected for a gas stream with high CO_2 concentration and small fractions of excessive O_2. This can be seen by the example in Fig. 8 for the combustion of CAL coal with Sinaus manganese ore as oxygen carrier using a specific solids inventory of

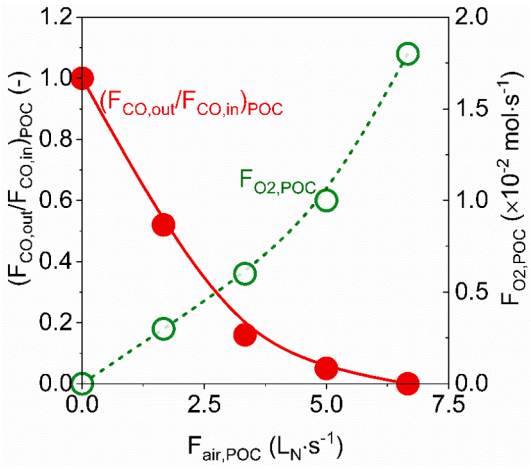

Fig. 8. Molar ratio of CO between the outlet and the inlet of the POC, $(F_{CO,out}/F_{CO,in})_{POC}$, and O_2 molar flow leaving the POC, $F_{O2,POC}$, under various $F_{air,POC}$ for a solids inventory of $m_{FR} = 550\ kg \cdot MW_{th}^{-1}$ during the combustion of CAL coal with Sinaus manganese ore.

$m_{FR} = 550\ kg \cdot MW_{th}^{-1}$ in the fuel reactor. In this case, the $(F_{CO,out}/F_{CO,in})_{POC}$ was decreased gradually from 1 to 0 as the POC air flow was increased from 0 to 6.7 L_N·s^{-1}, with a surplus O_2 flow of 0–1.8·10^{-2} mol·s^{-1} at the POC exit. Clearly, the air addition must be optimized to fulfill the requirement for the post treatment, e.g. transport and storage, of fuel-reactor gas stream in a scaled-up CLC system.

4.7. Conversion of combustible gases versus oxygen concentration

In order to compare among different solid fuels and operation conditions, the measured concentration of CH_4, CO and H_2 from POC was normalized using Eq. (6), which in combination with the overall oxygen ratio $\lambda_{O,overall}$ calculated by Eq. (7) are shown in Fig. 9 as a function of normalized O_2 concentration at the POC outlet. An increase of normalized O_2 concentration at the outlet of POC is a result of a higher excess of air O_2 introduced to the POC, which contributes to a larger numerator in Eq. (7), thus an increase in the overall oxygen ratio is seen in Fig. 9. As observed, the increase of normalized O_2 concentration can lead to a linear-like increase of the overall oxygen ratio, which means a higher availability of O_2 for oxidation and more contacts of O_2 and combustibles in the POC. In this case, lower normalized concentration of CH_4, CO and H_2 were obtained under higher values of normalized O_2 concentration or overall oxygen ratio. In the case of CH_4 in Fig. 9(a), the normalized CH_4 concentration was decreased from 0.087 to 0 while the overall oxygen ratio was raised from 0.80 to 1.05 as a function of normalized O_2 concentration. For the CO in Fig. 9(b), the highest normalized concentration was 0.16 for BP pellets. Full or almost full oxidation of CO can be realized with $x_{O2,N} > 0.01$ and $\lambda_{O,overall} > 1.01$. For the case of H_2 in Fig. 9(c), again the higher normalized O_2 concentration led to an increase on the overall oxygen ratio, which resulted in more available O_2 and more opportunities for the contact of O_2 and H_2 in the POC, thus a lower normalized H_2 concentration was obtained. However, a complete oxidation of H_2 cannot be seen in Fig. 9(c), because few tests were done with the H_2 concentration in POC being measured. Generally, in any case of Fig. (9), it was found that a higher overall oxygen ratio can help to reach a higher extent of fuel combustion in the POC reactor. Nevertheless, too high overall oxygen ratio can also reduce the purity of CO_2 due to the excess of O_2, thereby, this parameter must be well optimized in a large-scale CLC system, e.g. by using pure O_2 and improving the POC design.

As can be seen in Fig. 9(b), there is some spread in the normalized CO concentration for a given normalized O_2 concentration in the outgoing stream of POC. The reason for this spread is not fully understood, but it is

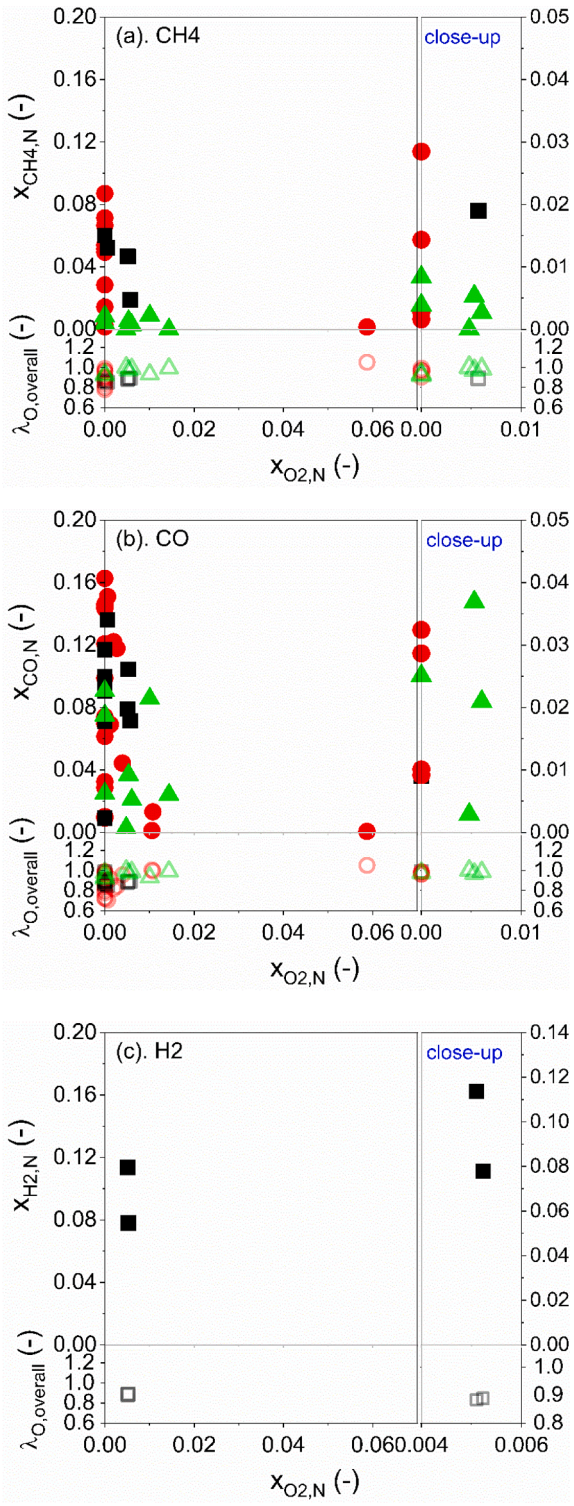

Fig. 9. Normalized concentration of (a) CH_4, (b) CO and (c) H_2 and the overall oxygen ratio, $\lambda_{O,overall}$, as a function of normalized O_2 concentration for the POC during the combustion of BP pellets (●, ○), GWC wood char (▲, △) and CAL coal (■, □), filled symbols for normalized gas concentration and void symbols for $\lambda_{O,overall}$; close-ups for details in the interval of $x_{O2,N} = 0$–0.01 for CH_4 and CO and in the interval of $x_{O2,N} = 0.004$–0.006 for H_2 are also shown; data from both SC and Sinaus manganese ores were used.

clear from the data that low O_2 and CO were attainable for all the three fuels, i.e. both $x_{O2,N}$ and $x_{CO,N}$ below around 0.01. Three such periods are presented in the following section.

4.8. Simultaneous low CH_4, CO and O_2 after the POC

Fig. 10, as an example, shows in detail the normalized concentration of CH_4, CO and O_2 reached after the POC under different air flow rates,

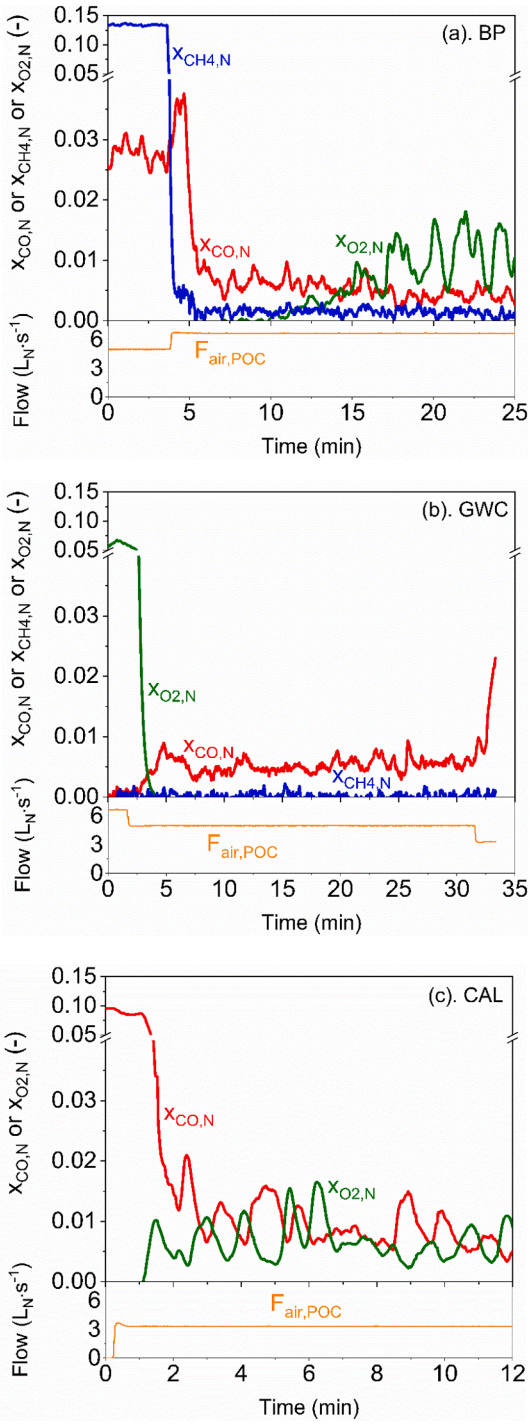

Fig. 10. Tests showing simultaneous low concentrations of O_2, CO and/or CH_4 at the outlet of POC using (a) 67 kW_{th} BP pellets with SC ore, (b) 80 kW_{th} GWC char with SC ore and (c) 65 kW_{th} CAL coal with Sinaus ore; CH_4 concentration was not measured for CAL and H_2 was not measured for all the three fuels for these results.

using the BP, GWC and CAL fuels. These cases were obtained after the flow of air to the POC was increased or decreased under stable fuel reactor operation with different thermal powers of fuel. Similar to that shown in Fig. 5, the increase of POC air flow led to a better combustion but also a dilution on gas concentration, while the opposite happened when decrease the POC air flow, which can also be clearly seen in Fig. 10. For each case, the variation of air flow to POC resulted in rapid increases or decreases of the normalized concentration of CH_4, CO and O_2 at the POC exit, which eventually converged to the desirable cases with relatively stable low concentrations. For the BP pellets in Fig. 10(a), with the air flow increased to around 6.7 $L_N \cdot s^{-1}$, the normalized concentration of CH_4 and CO was greatly lowered, while a gradual increase of O_2 is observed. After stabilization, low average normalized concentration of 0.5% for CO, 0.1% for CH_4 and 0.7% for O_2 was achieved with a duration of around 10 min before another test was conducted at $t = 25$ min. Similarly, an average normalized concentration of 0.5% CO was also reached in the cases of GWC char and CAL coal, see Fig. 10(b) and (c). For the GWC char, the low normalized CO concentration was reached with an air flow of around 5 $L_N \cdot s^{-1}$, while an O_2 concentration of zero was calculated. Also, CH_4 was zero, which is reasonable considering the lower fraction of methane entering the POC due to the low content of volatiles in this fuel. For CAL coal, the low CO was attained under an average normalized O_2 concentration of 0.5% in Fig. 10(c) using 3.3 $L_N \cdot s^{-1}$ air flowing to the POC. These experimental results in Fig. 10 confirm that a good conversion of combustibles from the fuel reactor can be realized in the POC unit of the 100 kW_{th} system with low excess of O_2, which is encouraging for the further optimization.

5. Discussion

5.1. Importance of lowering the char elutriation from fuel reactor

From the gas leaving the POC, it can be identified which combustible component is more dominant. As shown in Fig. 11, the comparison of normalized concentration indicates that CO is normally present in similar or higher concentration than CH_4 and H_2. The normalized concentration of CH_4 were always lower than CO, whereas only two measurements were available for H_2. Nevertheless, H_2 is generally easier to burn than CO, thus, with sufficient air addition H_2 should be lower. For CH_4, the dependence on fuel type is also observed in Fig. 11 and clearly related to the different volatiles fractions as discussed before. As can be seen from Fig. 10(a), the oxygen addition removes CH_4 much more efficiently as compared to CO. This might be related to the partial post-oxidation of elutriated char to CO in the POC unit. As is noticed in Fig. 5 (c), air addition, if not sufficient, may substantially increase the flow of CO as a result of inadequate combustion of elutriated char. Thus, it is also possible that char may contribute to CO even under well optimized conditions. The fuel with the highest char elutriation in this work, i.e. CAL coal, also shows somewhat higher $CO + O_2$ in Fig. 10. Accordingly, fuel properties and reactor system giving a much lower content of unburnt char in the fuel reactor stream are expected to facilitate high conversion in the oxy-polishing step.

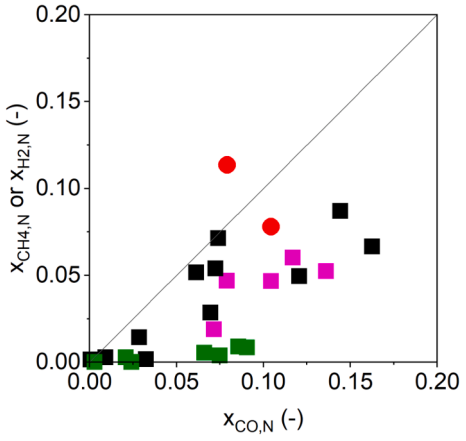

Fig. 11. Normalized concentration of CH_4 (cubic symbols: ■, ■, ■) and H_2 (circle symbols: ●) in comparison with normalized CO concentration at the POC outlet for BP pellets (■, ●), GWC wood char (■) and CAL coal (■) using the SC and Sinaus manganese ores as oxygen carrier.

5.2. Options for improving the POC performance

Using a typical average fuel-reactor gas composition (10.1 vol% CO, 5.0 vol% CH_4, 7.2 vol% H_2 and 52.9 vol% CO_2), the POC was simulated at 880 °C, under various air or pure O_2 flows, with the zero-dimensional model described in *Section 2.5* and the results are presented in Fig. 12. In comparison with the POC experiments, the model shows reasonably good predictions for the best conversions, i.e. most cases for CH_4 and two cases for CO. Given the spread in the experimental results, the model cannot at the same time predict the lower conversions seen for the remaining data. The latter can be attributed to the residual fuel-reactor char, the uncertainty of measurements and the variations in experimental conditions, e.g. temperature in the POC. The unconverted char from the fuel reactor is expected to be partly oxidized to CO in the POC, and this unknown flow of char was not included in the model. There is no comparison of H_2 concentration and model because the number of measurements for this component is very limited in the experiments. Using pure O_2 stream in the model, the combustibles can be further lowered at the same normalized O_2 concentrations. The model predicts it would be possible to reach a fraction of combustibles plus O_2, i.e. $CO + CH_4 + H_2 + O_2$, below 0.009 with air and 0.006 with pure O_2.

In a scaled-up system, the oxy-polishing step would have an O_2 gas flow not diluted by nitrogen, which raises the POC oxidation capability and should improve the combustion (see Fig. 12), in particular, as it would also raise the temperature. With no air nitrogen present to form NO_x, a high POC temperature should have no significant disadvantage. Furthermore, a considerably lower char elutriation is expected in larger systems due to the higher reactor height and a better separation by the cyclone. However, it would only be possible to reach low O_2 and low combustibles with a good mixing of the gases in the POC.

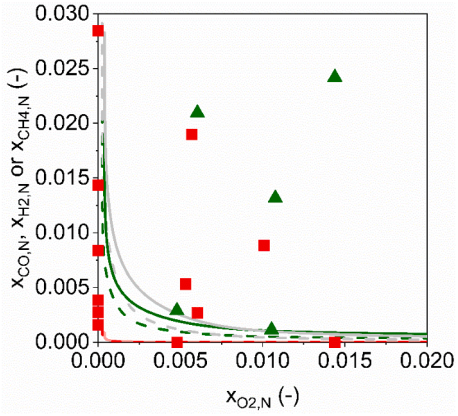

Fig. 12. Model and experimental results for the POC in terms of the normalized concentration of CH_4 (■, —, - -), CO (▲, —, - -) and H_2 (—, - -) as a function of normalized O_2 concentration at the outlet of POC and the third CSTR; symbols (■, ▲) are for experimental data, continuous lines (—, —, —) represent the modeling data with air as oxidization agent and dash lines (- -, - -, - -) show the modeling data using a pure O_2 stream.

6. Conclusions

Oxy-polishing step for Chemical Looping Combustion (CLC) process was demonstrated with a post-oxidation chamber (POC) of the 100 kW_{th} prototype using three different solid fuels and two manganese ores as oxygen carrier. Operational conditions in the fuel reactor and the POC were changed in a wide range to study the performance of the oxy-polishing process. The following findings were made.

(i) The oxy-polishing step is feasible and important for getting a high purity CO_2 stream in the CLC process, which is advantageous for further gas conditioning before transport and storage. Using the POC, the gas conversion can be greatly improved from 0.887 to 0.894 after the fuel reactor to 0.993–0.997 at POC exit.
(ii) Fuel conversion in the POC is linked to the combustion behavior in the fuel reactor. Improving the fuel reactor combustion, the POC performance can be enhanced. Also, the conditions in POC can also be optimized by varying the addition of oxygen.
(iii) A trade-off was found in the POC between the fuel conversion and the excess of O_2. By tuning the overall oxygen ratio to slightly higher than 1.01, an operation close to optimum was realized with only minor oxygen excess and simultaneous low fractions of CO and O_2 below 0.5–1.0%.
(iv) Removal of CH_4 by the POC is more efficient than removal of CO, which might be caused by the slow oxidation of fuel-reactor char in the POC. Lowering the char elutriation from the fuel reactor is expected to lead to a better oxy-polishing combustion.
(v) Performance of the POC was compared to a simple reactor model, indicating the potential of using modeling to guide the future scale-up design. The model shows improved POC performance when using pure O_2 stream as oxidation agent.

Declaration of Competing Interest

The authors declare that they have no known competing financial interests or personal relationships that could have appeared to influence the work reported in this paper.

Acknowledgements

This work was carried out as part of the OxyCar-FBC project, which is conducted within the framework of ERA-NET Bioenergy and funded by the Swedish Energy Agency (P43936-1) and the "Negative CO_2" project funded by Nordic Energy Research.

References

[1] International Energy Agency, Energy Technology Perspectives 2017, OECD/IEA, Paris, 2017.
[2] A. Lyngfelt, A. Brink, Ø. Langørgen, T. Mattisson, M. Rydén, C. Linderholm, 11,000 h of chemical-looping combustion operation—Where are we and where do we want to go? Int. J. Greenhouse Gas Control 88 (2019) 38–56.
[3] J. Adánez, A. Abad, T. Mendiara, P. Gayán, L.F. de Diego, F. García-Labiano, Chemical looping combustion of solid fuels, Prog. Energy Combust. Sci. 65 (2018) 6–66.
[4] A. Lyngfelt, Chemical Looping Combustion: Status and Development Challenges, Energy Fuels 34 (8) (2020) 9077–9093.
[5] T. Mendiara, F. García-Labiano, A. Abad, P. Gayán, L.F. de Diego, M.T. Izquierdo, J. Adánez, Negative CO_2 emissions through the use of biofuels in chemical looping technology: A review, Appl. Energy 232 (2018) 657–684.
[6] A. Lyngfelt, B.o. Leckner, A 1000 MW_{th} boiler for chemical-looping combustion of solid fuels – Discussion of design and costs, Appl. Energy 157 (2015) 475–487.
[7] A. Lyngfelt, Chemical-looping combustion of solid fuels – Status of development, Appl. Energy 113 (2014) 1869–1873.
[8] A. Lyngfelt, M. Johansson, T. Mattisson, Chemical-looping combustion-status of development, 9th International Conference on Circulating Fluidized Beds, Hamburg, Germany, 2008.
[9] M. Rydén, P. Moldenhauer, T. Mattisson, A. Lyngfelt, M. Younes, T. Niass, B. Fadhel, J.-P. Ballaguet, Chemical-Looping Combustion with Liquid Fuels, Energy Procedia 37 (2013) 654–661.
[10] J. Adanez, A. Abad, F. Garcia-Labiano, P. Gayan, L.F. de Diego, Progress in Chemical-Looping Combustion and Reforming technologies, Prog. Energy Combust. Sci. 38 (2) (2012) 215–282.
[11] T. Mattisson, M. Keller, C. Linderholm, P. Moldenhauer, M. Rydén, H. Leion, A. Lyngfelt, Chemical-looping technologies using circulating fluidized bed systems: Status of development, Fuel Process. Technol. 172 (2018) 1–12.
[12] H.e. Fang, L.i. Haibin, Z. Zengli, Advancements in Development of Chemical-Looping Combustion: A Review, Int. J. Chem. Eng. 2009 (2009) 1–16.
[13] A. Lyngfelt, B. Leckner, T. Mattisson, A fluidized-bed combustion process with inherent CO_2 separation: application of chemical-looping combustion, Chem. Eng. Sci. 56 (2001) 3101–3113.
[14] H.R. Kerr, Chapter 38 - Capture and Separation Technology Gaps and Priority Research Needs, in: D.C. Thomas (Ed.), Carbon Dioxide Capture for Storage in Deep Geologic Formations, Elsevier Science, Amsterdam, 2005, pp. 655–660.
[15] H. Zhao, X. Tian, J. Ma, M. Su, B. Wang, D. Mei, Development of tailor-made oxygen carriers and reactors for chemical looping processes at Huazhong University of Science & Technology, Int. J. Greenhouse Gas Control. 93 (2020), 102898.
[16] A. Thon, M. Kramp, E.-U. Hartge, S. Heinrich, J. Werther, Operational experience with a system of coupled fluidized beds for chemical looping combustion of solid fuels using ilmenite as oxygen carrier, Appl. Energy 118 (2014) 309–317.
[17] M. Schmitz, C. Linderholm, Chemical looping combustion of biomass in 10- and 100-kW pilots – Analysis of conversion and lifetime using a sintered manganese ore, Fuel 231 (2018) 73–84.
[18] P. Markström, C. Linderholm, A. Lyngfelt, Operation of a 100 kW chemical-looping combustor with Mexican petroleum coke and Cerrejón coal, Appl. Energy 113 (2014) 1830–1835.
[19] H.u. Chen, M. Cheng, L. Liu, Y.e. Li, Z. Li, N. Cai, Coal-fired chemical looping combustion coupled with a high-efficiency annular carbon stripper, Int. J. Greenhouse Gas Control 93 (2020) 102889, https://doi.org/10.1016/j.ijggc.2019.102889.
[20] A. Abad, J. Adánez, P. Gayán, L.F. de Diego, F. García-Labiano, G. Sprachmann, Conceptual design of a 100 MW_{th} CLC unit for solid fuel combustion, Appl. Energy 157 (2015) 462–474.
[21] T. Song, L. Shen, Review of reactor for chemical looping combustion of solid fuels, Int. J. Greenhouse Gas Control 76 (2018) 92–110.
[22] K. Marx, J. Bolhàr-Nordenkampf, T. Pröll, H. Hofbauer, Chemical looping combustion for power generation—Concept study for a 10MW_{th} demonstration plant, Int. J. Greenhouse Gas Control 5 (5) (2011) 1199–1205.
[23] M. Schmitz, C.J. Linderholm, A. Lyngfelt, Chemical looping combustion of four different solid fuels using a manganese-silicon-titanium oxygen carrier, Int. J. Greenhouse Gas Control 70 (2018) 88–96.
[24] D. Karami, A.H. Soleimanisalim, M.H. Sedghkerdar, N. Mahinpey, Preparation of Novel Oxygen Carriers Supported by Ti, Zr-Shelled γ-Alumina for Chemical Looping Combustion of Methane, Ind. Eng. Chem. Res. 59 (7) (2020) 3221–3228.
[25] B. Wang, H. Li, Y. Liang, L. Lv, D. Mei, N. Ding, H. Zhao, Chemical Looping Combustion Characteristics of Coal with a Novel CaSO 4 –Ca 2 CuO 3 Mixed Oxygen Carrier, Energy Fuels 34 (6) (2020) 7316–7328.
[26] H. Zhao, X. Tian, J. Ma, X. Chen, M. Su, C. Zheng, Y. Wang, Chemical Looping Combustion of Coal in China: Comprehensive Progress Remaining Challenges, and Potential Opportunities, Energy Fuels 34 (2020) 6696–6734.
[27] J. Adánez, A. Abad, Chemical-looping combustion: Status and research needs, Proc. Combust. Inst. 37 (4) (2019) 4303–4317.
[28] A. Abad, J. Adánez, L.F. de Diego, P. Gayán, F. García-Labiano, A. Lyngfelt, Fuel reactor model validation: Assessment of the key parameters affecting the chemical-looping combustion of coal, Int. J. Greenhouse Gas Control 19 (2013) 541–551.
[29] P. Gayán, A. Abad, L.F. de Diego, F. García-Labiano, J. Adánez, Assessment of technological solutions for improving chemical looping combustion of solid fuels with CO_2 capture, Chem. Eng. J. 233 (2013) 56–69.
[30] A. Pérez-Astray, T. Mendiara, L.F. de Diego, A. Abad, F. García-Labiano, M. T. Izquierdo, J. Adánez, Improving the oxygen demand in biomass CLC using manganese ores, Fuel 274 (2020) 117803, https://doi.org/10.1016/j.fuel.2020.117803.
[31] R. Pérez-Vega, A. Abad, J.A. Bueno, F. García-Labiano, P. Gayán, L.F. de Diego, J. Adánez, Improving the efficiency of Chemical Looping Combustion with coal by using ring-type internals in the fuel reactor, Fuel 250 (2019) 8–16.
[32] D.C. Guío-Pérez, H. Hofbauer, T. Pröll, Effect of ring-type internals on solids distribution in a dual circulating fluidized bed system-cold flow model study, AIChE J. 59 (10) (2013) 3612–3623.
[33] V. Kempkes, A. Kather, Chemical looping combustion: comparative analysis of two different overall process configurations for removing unburnt gaseous components, 2nd International Conference on Chemical Looping, Darmstadt, Germany, 2012.
[34] C. Linderholm, A. Lyngfelt, A. Cuadrat, E. Jerndal, Chemical-looping combustion of solid fuels – Operation in a 10kW unit with two fuels, above-bed and in-bed fuel feed and two oxygen carriers, manganese ore and ilmenite, Fuel 102 (2012) 808–822.
[35] J. Yan, L. Shen, S. Jiang, J. Wu, T. Shen, T. Song, Combustion Performance of Sewage Sludge in a Novel CLC System with a Two-Stage Fuel Reactor, Energy Fuels 31 (11) (2017) 12570–12581.
[36] J. Haus, K. Lyu, E.-U. Hartge, S. Heinrich, J. Werther, Analysis of a Two-Stage Fuel Reactor System for the Chemical-Looping Combustion of Lignite and Bituminous Coal, Energy Technol. 4 (10) (2016) 1263–1273.
[37] D. Mei, A. Abad, H. Zhao, S. Yan, B. Wang, Q. Yuan, Extension and evaluation of a macroscopic model for syngas-fueled chemical looping combustion, Chem. Eng. Process. Process Intensif. 133 (2018) 106–116.

[38] F. García-Labiano, J. Adánez, L.F. de Diego, P. Gayán, A. Abad, Effect of Pressure on the Behavior of Copper-, Iron-, and Nickel-Based Oxygen Carriers for Chemical-Looping Combustion, Energy Fuels 20 (1) (2006) 26–33.
[39] D. Mei, H. Zhao, S. Yan, Kinetics model for the reduction of Fe 2 O 3 /Al 2 O 3 by CO in Chemical Looping Combustion, Chem. Eng. Process. Process Intensif. 124 (2018) 137–146.
[40] S. Zhang, C. Saha, Y. Yang, S. Bhattacharya, R. Xiao, Use of Fe_2O_3-Containing Industrial Wastes As the Oxygen Carrier for Chemical-Looping Combustion of Coal: Effects of Pressure and Cycles, Energy Fuels 25 (2011) 4357–4366.
[41] Y.e. Li, Z. Li, L. Liu, N. Cai, Measuring the fast oxidation kinetics of a manganese oxygen carrier using microfluidized bed thermogravimetric analysis, Chem. Eng. J. 385 (2020) 123970, https://doi.org/10.1016/j.cej.2019.123970.
[42] T. Mendiara, L.F. de Diego, F. García-Labiano, P. Gayán, A. Abad, J. Adánez, On the use of a highly reactive iron ore in Chemical Looping Combustion of different coals, Fuel 126 (2014) 239–249.
[43] D. Mei, T. Mendiara, A. Abad, L.F. de Diego, F. García-Labiano, P. Gayán, J. Adánez, H. Zhao, Manganese Minerals as Oxygen Carriers for Chemical Looping Combustion of Coal, Ind. Eng. Chem. Res. 55 (22) (2016) 6539–6546.
[44] I. Gogolev, C. Linderholm, D. Gall, M. Schmitz, T. Mattisson, J.B.C. Pettersson, A. Lyngfelt, Chemical-looping combustion in a 100 kW unit using a mixture of synthetic and natural oxygen carriers – Operational results and fate of biomass fuel alkali, Int. J. Greenhouse Gas Control 88 (2019) 371–382.
[45] A. Cuadrat, A. Abad, F. García-Labiano, P. Gayán, L.F. de Diego, J. Adánez, Relevance of the coal rank on the performance of the in situ gasification chemical-looping combustion, Chem. Eng. J. 195-196 (2012) 91–102.
[46] N. Berguerand, A. Lyngfelt, Design and operation of a $10kW_{th}$ chemical-looping combustor for solid fuels – Testing with South African coal, Fuel 87 (12) (2008) 2713–2726.
[47] P.C. Wankat, K.P. Kostroski†, Hybrid Air Separation Processes for Production of Oxygen and Nitrogen, Sep. Sci. Technol. 45 (9) (2010) 1171–1185.
[48] O. Authier, Y. Le Moullec, Coal Chemical-Looping Combustion for Electricity Generation: Investigation for a 250 MW_e Power Plant, Energy Procedia 37 (2013) 588–597.
[49] C. Linderholm, M. Schmitz, M. Biermann, M. Hanning, A. Lyngfelt, Chemical-looping combustion of solid fuel in a 100 kW unit using sintered manganese ore as oxygen carrier, Int. J. Greenhouse Gas Control 65 (2017) 170–181.
[50] C. Linderholm, P. Knutsson, M. Schmitz, P. Markström, A. Lyngfelt, Material balances of carbon, sulfur, nitrogen and ilmenite in a 100kW CLC reactor system, Int. J. Greenhouse Gas Control 27 (2014) 188–202.
[51] J. Ströhle, M. Orth, B. Epple, Design and operation of a 1 M_{Wt}h chemical looping plant, Appl. Energy 113 (2014) 1490–1495.
[52] P. Ohlemüller, J.-P. Busch, M. Reitz, J. Ströhle, B. Epple, 2016. Chemical-Looping Combustion of Hard Coal: Autothermal Operation of a 1 MWth Pilot Plant. J. Energy Resour. Technol. 138, 042203.
[53] M. Keller, H. Leion, T. Mattisson, Mechanisms of Solid Fuel Conversion by Chemical-Looping Combustion (CLC) using Manganese Ore: Catalytic Gasification by Potassium Compounds, Energy Technol. 1 (2013) 273–282.
[54] International Organization for Standardization. ISO 3923-1:2018 Metallic powders — Determination of apparent density — Part 1: Funnel method, 2018.
[55] M. Rydén, P. Moldenhauer, S. Lindqvist, T. Mattisson, A. Lyngfelt, Measuring attrition resistance of oxygen carrier particles for chemical looping combustion with a customized jet cup, Powder Technol. 256 (2014) 75–86.
[56] S. Sundqvist, M. Arjmand, T. Mattisson, M. Rydén, A. Lyngfelt, Screening of different manganese ores for chemical-looping combustion (CLC) and chemical-looping with oxygen uncoupling (CLOU), Int. J. Greenhouse Gas Control 43 (2015) 179–188.
[57] S. Sundqvist, T. Mattisson, H. Leion, A. Lyngfelt, Oxygen release from manganese ores relevant for chemical looping with oxygen uncoupling conditions, Fuel 232 (2018) 693–703.
[58] International Organization for Standardization. ISO 17246:2010 Coal — Proximate analysis, 2010.
[59] ASTM International, D5373–02 Standard Test Methods for Instrumental Determination of Carbon, Hydrogen, and Nitrogen in Laboratory Samples of Coal and Coke, PA; ASTM International, West Conshohocken, 2002.
[60] P. Markström, C. Linderholm, A. Lyngfelt, Chemical-looping combustion of solid fuels – Design and operation of a 100kW unit with bituminous coal, Int. J. Greenhouse Gas Control 15 (2013) 150–162.
[61] C. Linderholm, M. Schmitz, A. Lyngfelt, Estimating the solids circulation rate in a 100-kW chemical looping combustor, Chem. Eng. Sci. 171 (2017) 351–359.
[62] D.G. Goodwin, R.L. Speth, H.K. Moffat, B.W. Weber, Cantera: An object-oriented software toolkit for chemical kinetics, thermodynamics, and transport processes. https://www.cantera.org, 2018. Version 2.4.0. doi:10.5281/zenodo.1174508.
[63] G.P. Smith, D.M. Golden, M. Frenklach, N.W. Moriarty, B. Eiteneer, M. Goldenberg, C.T. Bowman, R.K. Hanson, S. Song, W.C. Gardiner, Jr., V.V. Lissianski, Z. Qin http://www.me.berkeley.edu/gri_mech/.
[64] Daofeng Mei, Alberto Abad, Haibo Zhao, Juan Adánez, Chuguang Zheng, On a Highly Reactive Fe 2 O 3 /Al 2 O 3 Oxygen Carrier for in Situ Gasification Chemical Looping Combustion, Energy Fuels 28 (11) (2014) 7043–7052.
[65] Jinchen Ma, Chaoquan Wang, Haibo Zhao, Xin Tian, Sulfur Fate during the Lignite Pyrolysis Process in a Chemical Looping Combustion Environment, Energy Fuels 32 (4) (2018) 4493–4501.